Quantification of Bound Microbubbles in Ultrasound Molecular Imaging

Verya Daeichin, Zeynettin Akkus, Ilya Skachkov, Klazina Kooiman, *Member, IEEE*, Andrew Needles, Judith Sluimer, Ben Janssen, Mat J. A. P. Daemen, Antonius F. W. van der Steen, *Fellow, IEEE*, Nico de Jong, *Member, IEEE*, and Johan G. Bosch, *Member, IEEE*

***Abstract*—Molecular markers associated with diseases can be visualized and quantified noninvasively with targeted ultrasound contrast agent (t-UCA) consisting of microbubbles (MBs) that can bind to specific molecular targets. Techniques used for quantifying t-UCA assume that all unbound MBs are taken out of the blood pool few minutes after injection and only MBs bound to the molecular markers remain. However, differences in physiology, diseases, and experimental conditions can increase the longevity of unbound MBs. In such conditions, unbound MBs will falsely be quantified as bound MBs. We have developed a novel technique to distinguish and classify bound from unbound MBs. In the post-processing steps, first, tissue motion was compensated using block-matching (BM) techniques. To preserve only stationary contrast signals, a minimum intensity projection (MinIP) or 20th-percentile intensity projection (PerIP) was applied. The after-flash MinIP or PerIP was subtracted from the before-flash MinIP or PerIP. In this way, tissue artifacts in contrast images were suppressed. In the next step, bound MB candidates were detected. Finally, detected objects were tracked to classify the candidates as unbound or bound MBs based on their displacement. This technique was validated *in vitro*, followed by two *in vivo* experiments in mice. Tumors ($n = 2$) and salivary glands of hypercholesterolemic mice ($n = 8$) were imaged using a commercially available scanner. Boluses of 100 μL of a commercially available t-UCA targeted to angiogenesis markers and untargeted control UCA were injected separately. Our results show considerable reduction in misclassification of unbound MBs as bound ones. Using our method, the ratio of bound MBs in salivary gland for images with targeted UCA versus control UCA was improved by up to two times compared with unprocessed images.**

Manuscript received February 8, 2015; accepted March 19, 2015. This research was supported by the Center for Translational Molecular Medicine and the Netherlands Heart Foundation (PARISk).

V. Daeichin, Z. Akkus, I. Skachkov, K. Kooiman, A. F. W. van der Steen, N. de Jong, and J. G. Bosch are with the Department of Biomedical Engineering, Thoraxcenter, Erasmus MC, 3000 CA Rotterdam, The Netherlands (e-mail: v.daeichin@erasmusmc.nl).

A. F. W. van der Steen is also with the Shenzhen Institute of Advanced Technologies, 518000 Shenzhen, China, and the Interuniversity Cardiology Institute of The Netherlands, 3511 EP Utrecht, The Netherlands.

N. de Jong is also with the Department of Imaging Science and Technology, Delft University of Technology, 2628 CJ Delft, the Netherlands, and the Interuniversity Cardiology Institute of The Netherlands, 3511 EP Utrecht, The Netherlands.

A. Needles is with VisualSonics Inc., Toronto, ON M4N 3N1, Canada.

J. Sluimer is with the Department of Pathology, Maastricht University Medical Centre (MUMC), 6229 HX Maastricht, The Netherlands.

B. Janssen is with the Department of Pharmacology, MUMC, 6229 HX Maastricht, The Netherlands.

M. J. A. P. Daemen is with the Department of Pathology, Academic Medical Center, 1105 AZ Amsterdam, The Netherlands.

DOI http://dx.doi.org/10.1109/TUFFC.2015.006264

I. Introduction

Molecular imaging with ultrasound using targeted ultrasound contrast agents (t-UCA) is a valuable tool that is being used increasingly for noninvasive quantification of angiogenesis [1]. Angiogenesis is known to be an essential marker of tumor growth and metastasis [2]. Various biomarkers associated with angiogenesis can be detected and quantified with different techniques such as positron emission tomography [3], magnetic resonance imaging [4], computed tomography [5], optical imaging [6], and ultrasonography using t-UCA [7]. Molecular imaging using t-UCA is a compelling imaging technique because it allows real-time monitoring of anatomy and functionality and it is inexpensive and portable [7]. This technique has been applied to characterize atherosclerosis [8], thrombosis [9], neovasculature [9], [10], lymph nodes [11], and inflammation [12], [13]. Also, ultrasound molecular imaging has been proven to be highly sensitive to the identification of molecular structures or expression when using t-UCA; thus, it provides helpful insights into genesis, progression, and prevention of diseases [14]–[18].

The most widely utilized methods for contrast ultrasound molecular imaging encompass injection of t-UCA followed by a waiting time (up to 10 min) to allow binding to targets and clearance of unbound microbubbles (u-MBs) from the blood. Consecutively, a combination of ultrasound imaging sequences and a high-power burst (flash) are applied, where the flash is used to destroy all MBs in the imaging plane. The intensity difference before and after the flash corresponds to the amount of bound MBs (b-MBs) which is a measure for molecular signals (we call this the classical approach in this manuscript) [10], [19]–[21]. In such methods, the quantification of b-MBs is strongly dependent on the injected t-UCA dose, imaging system gain, local perfusion [22], and the physiology and the state of the animal. However, in many conditions such as presence of tissue motion, high concentration of freely recirculating u-MBs after the waiting period, limited number of recorded frames, low frame rates, and small region of interest (ROI), such classical methods will not result in reliable quantification of b-MBs. Moreover, because these techniques are strongly dependent on imaging system settings, comparisons between different studies performed with different imaging settings are not yet possible.

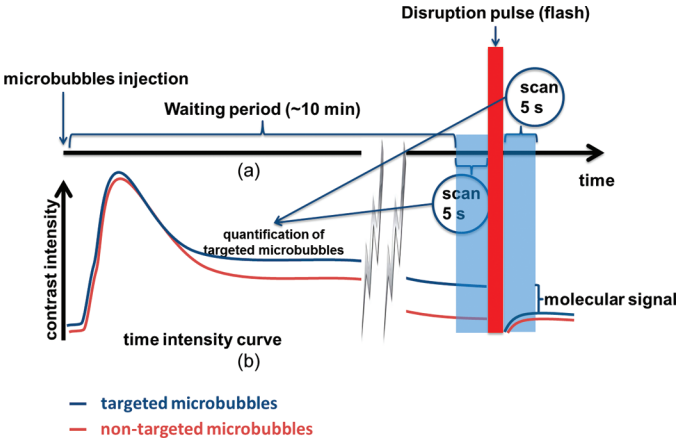

Fig. 1. (a) Timeline of the imaging protocol and (b) schematic representation of a typical time–intensity curve in the region of interest (e.g., salivary gland) corresponding to the timeline [intensity level for targeted microbubbles is slightly shifted from non-targeted (control) microbubbles for better illustration].

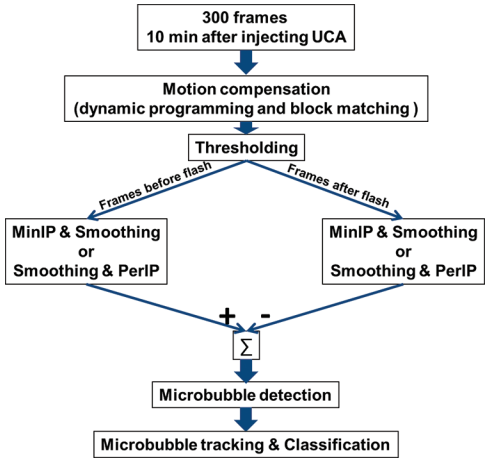

Fig. 2. Flowchart showing the steps of our technique for the quantification and classification of bound targeted microbubbles.

We have developed a new quantification method which benefits from motion compensation and individual contrast spot detection, and is capable of distinguishing the b-MB from u-MB based on their displacement. Our quantification method can be applied in studies performed with different imaging settings because it is less sensitive to imaging parameters. Moreover, it is more robust to tissue motion artifacts.

II. Methods

A high-frequency preclinical ultrasound scanner was operated at 18 MHz, with a 256-element linear-array transducer (Vevo 2100 with MS250 probe, VisualSonics Inc., Toronto, ON, Canada). The used MS250 probe has a center frequency of 22.5 MHz and a −6-dB two-way bandwidth of 70% (15 to 30 MHz) [23]. The transducer operated at 10% transmit power (~400 kPa at the focus of the probe, MI of 0.1) in the contrast mode and wide beam-width setting was chosen to have a low, uniform transmit pressure over depth. Side-by-side B-mode and nonlinear contrast mode images were acquired with a frame rate of 30 to 40 frames per second. Nonlinear fundamental imaging with amplitude modulation [23] was used for the contrast images. Lossless DICOM (digital imaging and communications in medicine) images were exported to Matlab (The MathWorks Inc., Natick, MA, USA) for further processing.

A. Imaging Protocol

Fig. 1(a) schematically shows a time sequence for molecular imaging in mice. After injecting the t-UCA, a waiting time of about 10 min is required for u-MBs to be taken out of the blood circulation by the lungs and liver. Also, this waiting period gives more time for the t-MBs to find the binding sites, thus increasing the number of t-MBs attached to the desired biomarker. After the 10-min waiting period, a series of about 300 frames (~10 s) was acquired with high-power bursts in the middle to disrupt all MBs in the imaging plane. A schematic representation of a typical time–intensity curve in the ROI is shown in Fig. 1(b) for two separate UCA injections (t-UCA in blue and non-targeted (control) UCA in red). Shortly after injecting the UCA, the intensity of contrast in the ROI increases rapidly, reaching a maximum and followed by a slow decay of intensity for both t-UCA and control UCA (c-UCA). However, because of the binding of the t-MBs to the targeted biomarkers in the ROI, the level of intensity, 10 min after the injection, will be higher for t-UCA than for c-UCA. Ideally, 10 min after injecting c-UCA, image intensity in the ROI should fall back to the baseline level (similar to the level before injection) and there should be no difference in image intensity before and after the flash pulse. On the other hand, there will be a difference in the intensity levels for t-UCA before and after the flash because of the b-MBs, which is a measure of the molecular signals in the ROI. Unfortunately, such an ideal situation will not always happen and even 10 min after injection there will be recirculating u-MBs for both t-UCA and c-UCA injections. Therefore, the actual difference in the intensity of the pre- and post-flash frames depends on the amount of both b-MBs and u-MBs the ROI. The increase in the intensity after the flash is also showing the presence of recirculating u-MBs.

B. Quantification Method

Subsets of the images captured 10 min after injecting the UCA were used for quantification of the b-MB in the ROI. The flowchart in Fig. 2 shows the steps of our quantification method.

Correction for tissue motion in the imaging plane was the first step of our technique. Akkus *et al.* [24] have developed an algorithm for tracking tissue motion for local contrast quantification using multidimensional dynamic programming (MDP) [25] combined with apodized block

matching (BM). This technique was adapted for the features of our DICOM images such as pixel size and intensity range and applied to the acquired images. The motion pattern of tissue in the ROI was extracted from B-mode images and applied to the contrast images to correct the motion of the ROI. In BM, a 60 × 40 (lateral × axial) pixel (2.4 × 1.6 mm) fixed template derived from the chosen B-mode image was scanned over a 60 × 20 (lateral × axial) pixel (2.4 × 0.8 mm) search field. Then, normalized correlation coefficients (NCC) for each 2-D displacement in each frame were used to construct a 3-D block of cost values. MDP was used to find the optimal 2-D tissue displacement path over time (the connective path in the time direction that had the highest sum of NCC values).

The noise levels in each data set were obtained by drawing an ROI in the background of a contrast frame immediately after the flash pulse and calculating the mean intensity value (μ) and standard deviation (σ) in the ROI. Then, all image intensities below a noise threshold level of $\mu + 4 \times \sigma$ were set to zero. In the next step, the motion-compensated contrast-mode frames were separated into two groups: pre-flash and post-flash. To show the effect of the number of frames on our quantification method, two subsets of images were chosen: a subset of 20 frames as the short sequence (10 frames each from pre- and post-flash groups); and a subset of 100 frames as the long sequence (50 frames each from pre- and post-flash groups). Next, a minimum intensity projection was applied on all the frames of each pre- and post-flash group resulting in a single minimum intensity projection (MinIP) image for each of these groups. The MinIP technique will collect per pixel the minimum intensity throughout all frames. In this way, the signal of nonstationary contrast spots will be minimized, because for each pixel the intensity will be low at some time point. Then, each of the single pre- and post-flash MinIP images were smoothened using a 2-D Gaussian filter of 3 × 3 pixels with $\sigma = 1$ to remove background noise (e.g., electronic noise). Objects smaller than the characteristic bubble size are removed with this filter. Because the MinIP step is a very radical step for removing the moving contrast spots which might also erroneously remove b-MBs, an alternative intensity projection step based on the 20th percentile of the intensity distribution per pixel over time (PerIP) was also applied instead of MinIP. The PerIP is more forgiving toward short-intensity variations or out-of-plane motion effects. The frames were smoothened using the same 2-D Gaussian filter before applying the PerIP. The resulting post-flash MinIP or PerIP images were subtracted from the pre-flash counterpart to reduce stationary artifacts and remaining tissue signal.

In the subtracted MinIP or PerIP images, individual contrast spots were detected using artificial bubble templates [26]. The templates mimic size and intensity pattern of contrast spots. Several radii (3, 5, and 7 pixels) of artificial bubbles were used for detection of different sizes of contrast spots. Each artificial template was scanned over the chosen ROI and normalized cross-correlation coefficients were calculated. In the resulting correlation coefficient matrix, the maximal correlation was located. After that, the correlation values in a 10 × 10 pixel-neighborhood around this location were set to zero. This was iteratively performed until the maximal correlation value was below 0.6, which is the threshold for a contrast spot to be considered as a bubble.

Ideally, after these processing steps, what should remain is the signal from the bound, stationary MBs that were destroyed by the flash. However, because of the low frame rate, the limited number of frames and also the high concentration of recirculating MBs, in some cases there will still be some u-MBs in the resulting image. Therefore further processing is required to classify the true b-MB from such u-MB. This was done by tracking all the detected MBs in the subset of 10 frames (short sequence) or 50 frames (long sequence) in the pre-flash image set. The tracking algorithm was based on MDP combined with BM as is described in [24], [26]. All the detected MBs with displacement less than 3 pixels (∼60 μm) were classified as stationary or b-MBs and the rest were discarded as u-MB.

In the classical approach, pre- and post-flash frames were averaged and subtracted from each other. Then, the total intensity in the subtracted image was calculated for a ROI and normalized to the area of the ROI. The results of the classical approach were compared with the results of our quantification method *in vivo*, using the same ROI in the subtracted MinIP and PerIP images.

C. In Vitro Experiment

An *in vitro* experiment was conducted to validate the ability of the MinIP and PerIP in reducing the u-MBs and also the classification step based on the single contrast spot detection and tracking. A thin layer (5 mm) of tissue-mimicking material (TMM) was prepared according to the recipe of Teirlinck *et al.* [27]. Target-ready UCAs were prepared from MicroMarker kit (VisualSonics Inc. Toronto, Canada) according the manufacturer's recipe. The TMM was placed at the bottom of a water tank filled with degassed water and a low concentration of MicroMarker was injected above the top of the material. The imaging probe (MS 250) was mounted 17 mm above the phantom and the focal zone was set at the top of the phantom. Then, side-by-side B-mode and contrast-mode images of MBs being pushed toward the phantom due to the radiation force were acquired. The imaging settings and acquisition protocol were similar to those used *in vivo*.

D. In Vivo Experiment

UCA were prepared as described for the *in vitro* experiment. MBs were targeted with biotinylated scVEGF (SibTech, Brookfield, CT, USA) or with biotinylated antibodies against $\alpha_v\beta_3$-integrin (BD Biosciences, San Jose, CA, USA) for making t-UCA. Inactive forms of biotinylated scVEGF (SibTech) and biotinylated IgG(κ) (BD Biosciences) were used for making the c-UCA.

First, well-vascularized subcutaneous Huh7 tumors with numerous targeting sites were imaged, for which the classical method shows good differences for targeted and control injections. Our method was compared with the classical method and validated in this model. Second, salivary glands as a model with weaker molecular signals were analyzed as a test of our method.

For the first experiment at Erasmus Medical Center, 8-week-old male NMRI nu/nu mice ($n = 2$) were purchased from Charles River Laboratories (Margate, UK) and fed *ad libitum*. Animals were kept under 2% isoflurane anesthesia and 5×10^6 Huh7 cells, a human hepatocellular carcinoma cell line, were injected in total volume of 100 μL in the right hind limb. When the tumor size reached 8 mm, animals were anesthetized with 2% isoflurane and placed on the Vevo Rail System heating stage (VisualSonics Inc.) and ultrasound imaging was performed. First, a bolus of 100 μL of control MicroMarker UCA was injected and 20 min after the first injection a bolus of 100 μL of t-UCA was injected via a tail vein catheter, with a flush of 0.9% saline after both injections. The injections were done using a programmable syringe pump (11 Pico Plus Elite, Harvard Apparatus, Kent, UK) with a rate of 600 μL per minute.

The second experiment was conducted at Maastricht University on hypercholesterolemic male ApoE knockout mice ($n = 8$) on a C57/BI6 background from an in-house breeding colony (originally from Iffa Credo, Lyon, France) and fed chow till the age of 50 weeks. Mice were anesthetized with ketamine (0.1 g/kg) and xylazine (0.02 g/kg) by subcutaneous injection and peri-operative ibuprofen (s.c.). Animals were intubated and artificially ventilated using room air at the rate of 160 strokes per minute. The left jugular vein was exposed, and a heat-stretched polyethylene-25 cannula was inserted (1.5 cm) and subcutaneously guided to the neck of the mouse. Here the catheter was fixed, extended, filled with heparinized saline (10 U/mL), and plugged. The rest of the experimental procedure was similar to the previous animals except that the UCA injections were done via the jugular vein cannula and the order of the injections was randomized in these animals. The right salivary gland was chosen as a target for this study, as it contains abundant neovascularization which expresses biomarkers to which our t-UCA could bind.

All animal work was approved by the regulatory authorities of Erasmus Medical Center and Maastricht University and performed in compliance with the Dutch government regulations.

III. Results

A. In Vitro Experiments

Fig. 3(a) shows a single frame of a B-mode recording of a layer of TMM (bright layer in the bottom of the image) and MBs floating above, in degassed water (bright spots floating in the dark background) . Because of the radiation force of the ultrasound, MBs were pushed toward the bottom, against the TMM layer. The MBs which were at the TMM layer from the beginning were not moving during the recorded frames, and therefore could be considered as stationary MBs. The MinIP images of the pre- and post- flash frames and their subtracted image for the short sequence (20 frames) are also shown in Figs. 3(b)–3(d). In Fig. 3(d), the stationary tissue signal was suppressed because it was present in both pre- and post-flash frames whereas the signals from the MBs were preserved in the subtraction step because they were destroyed by the flash and were not present in the post-flash frames.

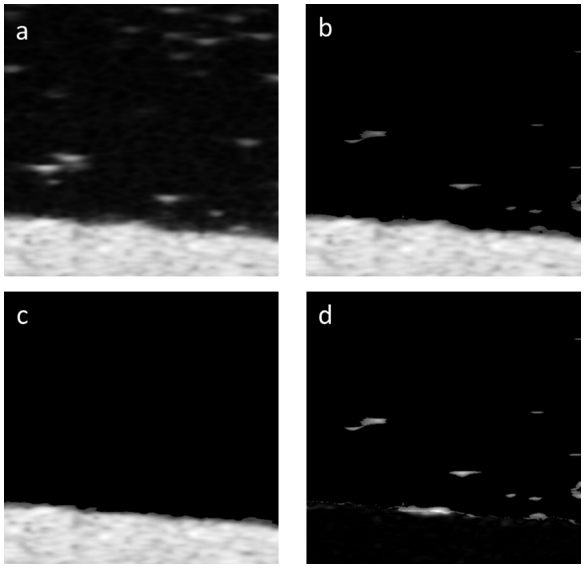

Fig. 3. *In vitro* validation experiment: (a) B-mode image, (b) MinIP of pre-flash B-mode frames (10 frames), (c) MinIP of post-flash B-mode frames (10 frames), and (d) their subtracted image.

MinIp and PerIP images were applied on short and long sequences and the results are depicted in Fig. 4. Some floating MBs were still preserved in both the MinIP and PerIP images when the short sequences were used [Figs. 4(a) and 4(b)] with a few more MBs in the PerIP image. However, when the long sequences were used all the floating MBs were suppressed in both the MinIP and PerIP images and only those stationary MBs just above the TMM layer were preserved [Figs. 4(c) and 4(d)].

The MB detection and tracking steps were applied on images of Figs. 4(a) and 4(b). All the detected MBs in the images were overlaid as red dots and indicated with white arrows in Figs. 4(a) and 4(b). All such detected contrast spots were tracked over all pre-flash frames in the short sequence (10 frames) and those with total motion less than 3 pixels were classified as stationary MBs and overlaid as yellow circles on these figures.

Four extra MBs were detected in the PerIP image [numbered from 1 to 4 in Fig. 4(b)] compared with the MinIP image. However, after tracking all the MBs and accepting only those which were moving less than 3 pixels [yellow circles in Figs. 4(a) and 4(b)], the same four stationary MBs were detected in both images.

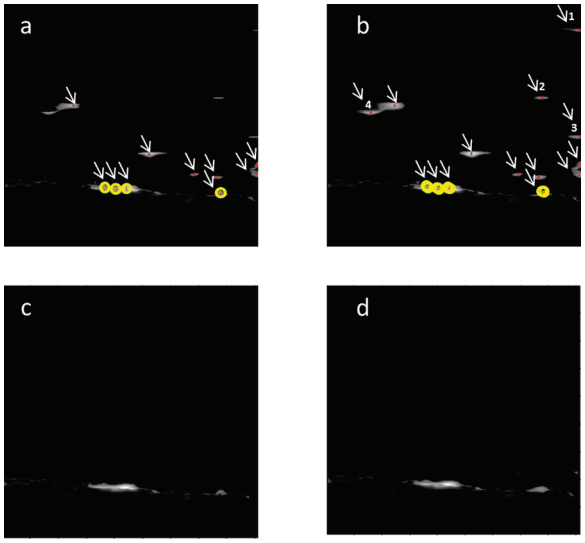

Fig. 4. Subtracted images after applying MinIP on (a) the short sequence and (c) the long sequence and after PerIP on (b) the short sequence and (d) the long sequence. In (a) and (b), detected microbubbles are overlaid as red dots and pointed out with white arrows and stationary microbubbles as yellow circles. Extra detected microbubbles in (b) are numbered.

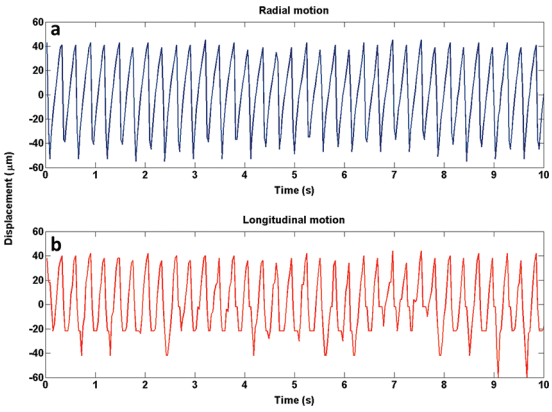

Fig. 5. Displacement of upper wall of right common carotid in radial (a) and longitudinal (b) directions in a mouse using automated motion tracking.

B. In Vivo Experiments

The motion compensation step is crucial *in vivo*, especially when fast-moving targets such as plaques in carotid artery walls are imaged. Fig. 5 shows the result of our motion tracking for a point on the upper wall of the right common carotid of a mouse in radial [Fig. 5(a)] and longitudinal [Fig. 5(b)] directions.

Our motion compensation method provides motion detection with a smallest step of 0.1 pixel. In general, it is more difficult to follow the longitudinal motion of the vessel because the speckle pattern of the wall tissue is very similar along the longitudinal direction. The error seen in Fig. 5(b) which looks like a quantization error is possibly caused by a shadow artifact in the image, hindering the tracking beyond a certain point.

Fig. 6 shows the result of our experiment on two tumors in B-mode [Figs. 6(a) and 6(d)] and contrast mode 10 min after injecting t-UCA [Figs. 6(b) and 6(e)] and c-UCA [Figs. 6(c) and 6(f)]. In both tumors, an enhanced intensity can be seen for the t-UCA [Figs. 6(b) and 6(e)] compared with the c-UCA [Figs. 6(c) and 6(f)].

Our quantification method and the classical approach were performed on the data set of these two tumors and the results are presented in Fig. 7. In both cases there are many b-MBs in the tumor for the targeted group and the difference between the targeted and control group is visible with the most commonly used classical approach. This confirms that our new method also gives good results in a situation with a high concentration of MBs and is similar to the classical method. The intensities obtained from the subtracted PerIP were less sensitive

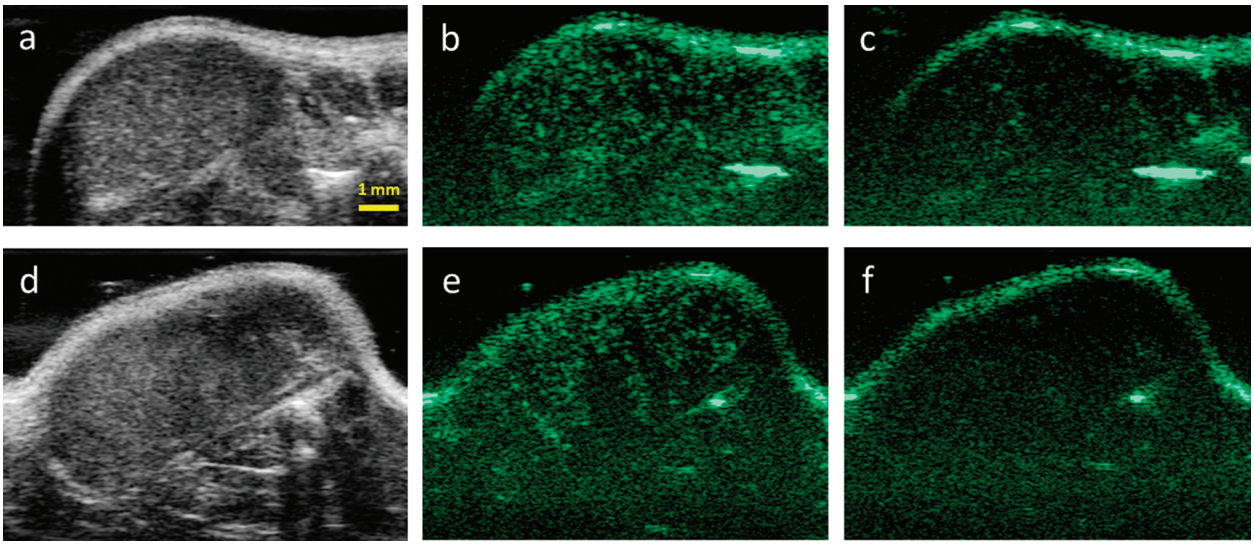

Fig. 6. (a and d) B-mode and (b–f) contrast mode ultrasound single frame images of two subcutaneous Huh7 liver tumors in two different mice (a, b, and c) tumor 1, (d, e, and f) tumor 2. (b and e) contrast mode images 10 min after injecting the targeted microbubbles. (c and f) contrast mode image 10 min after injecting the control microbubbles.

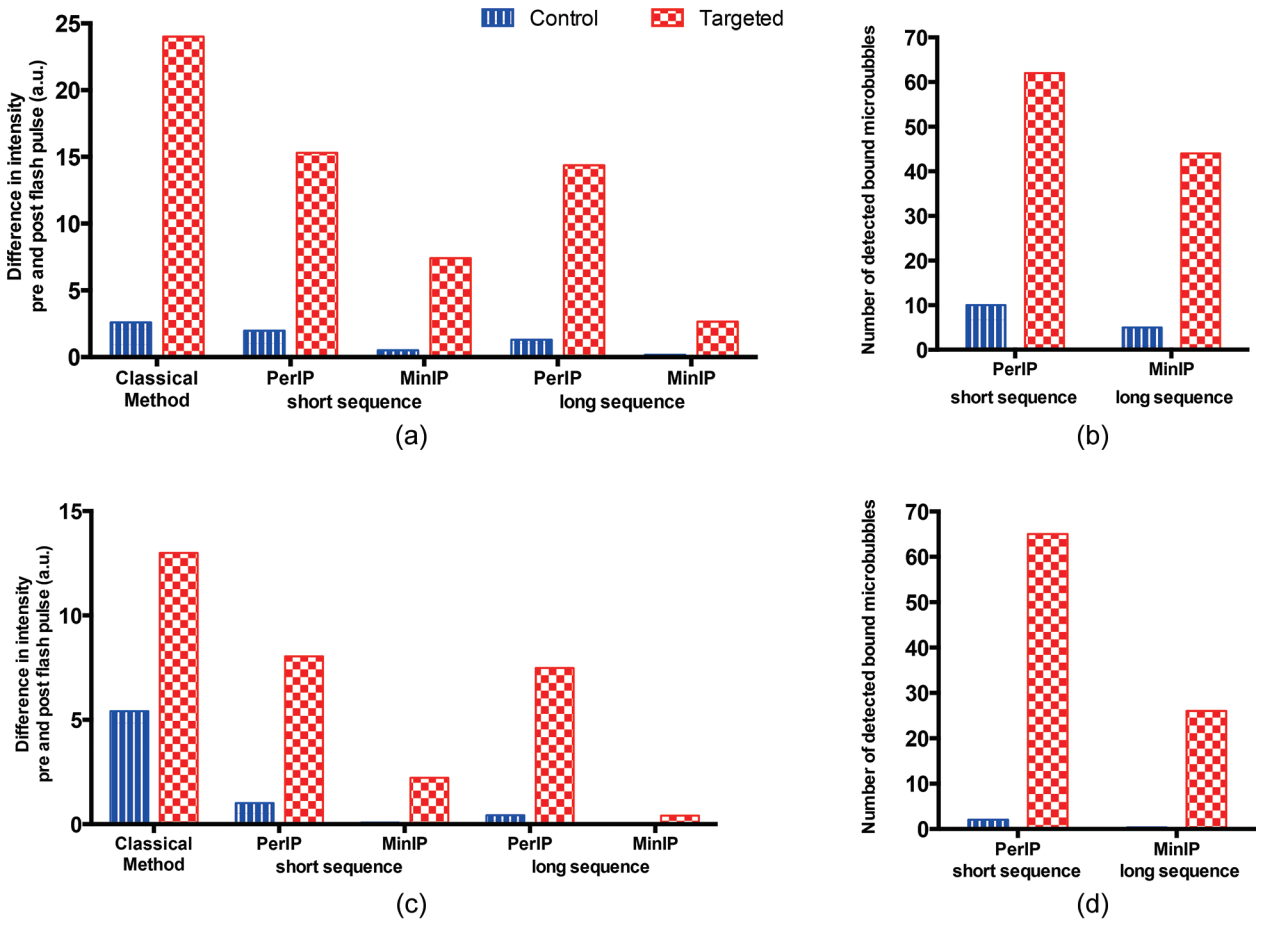

Fig. 7. Comparison of bound microbubbles quantifications on two tumors (a and b) tumor 1, (c and d) tumor 2. (a and c) Differences of pre- and post-flash image intensities in two tumors according to the classical subtraction method compared with differences of image intensities after applying MinIP and alternative intensity projection based on the PerIP and (b and d) number of detected bound microbubbles after performing our method on short and long sequences.

to the number of frames used in the analysis. The intensity in the subtracted MinIP image for the long sequence was about three times lower than for the short sequence. After tracking and classifying the detected MBs in both the subtracted MinIP and PerIP images, the number of detected b-MBs are shown in Figs. 7(b) and 7(d). These results were in very good agreement with what we visually saw in these tumors and also with the results of the classical method.

For the second *in vivo* experiment on salivary glands, 7 mice out of 8 showed successful targeting; see Fig. 8. The intensities within the salivary glands for these 7 mice were quantified using the classical method for the t-UCA and c-UCA injections. Also, the numbers of detected b-MBs using our method were calculated for these two injections for the short sequences. The ratio of intensities and the ratio of number of b-MBs in the targeted group over the control group for these 7 mice are presented as boxplots in Fig. 9. The boxplots in Fig. 9 show that the classical quantification approach does not show a big difference between the targeted and control injections. In contrast, our technique, which detects the number of b-MBs, clearly enhances the difference between these two injections. Also, a higher mean ratio in these 7 animals was observed when the MinIP is used compared with when PerIP is used.

IV. Discussion

We have developed a method which detects single contrast spots and classifies them into bound and unbound MBs based on their displacement in the recorded frames. The processing steps such as motion compensation and MinIP or PerIP assure that artifacts resulting from the motion of the ROI are minimized and only the stationary contrast spots are enhanced. In an *in vitro* setup, we showed that applying the MinIP or PerIP is sufficient to discard the u-MBs in the image if the recorded sequences are long enough (50 frames for each pre- and post-flash group). However, because of the limited number of recorded frames, limited frame rate, motion artifacts, complex *in vivo* conditions and variations in the concentration of remaining u-MBs in animals, the MB detection, tracking and classification steps will be beneficial *in vivo* (Figs. 6–9). Additionally, quantification of the molecular signals as number of b-MBs instead of image intensities is less de-

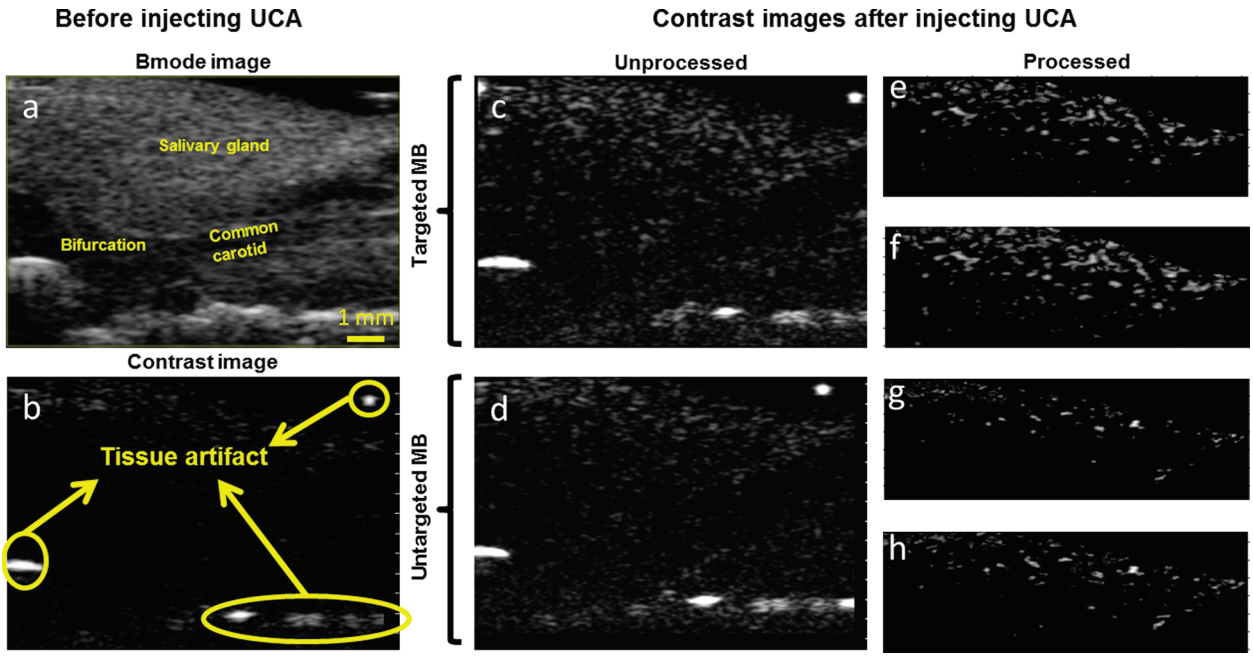

Fig. 8. (a) B-mode and (b–d) contrast mode ultrasound images of right salivary gland and right carotid including the bifurcation of an ApoE −/−, 50-week-old mouse. (b) the contrast mode before injecting the UCA, (c and d): single frame unprocessed images 10 min after injecting (c) targeted and (d) control microbubbles and their corresponding processed images for salivary gland by (e and g) MinIP and (f and h) PerIP. All the bright spots in the (e)–(h) images are contrast signals.

pendent on imaging settings and therefore more valuable for comparison and longitudinal studies.

The PerIP step was tested as an alternative to MinIP, because in the MinIP contrast spots will be disqualified even if they disappear in a single frame of the sequence, e.g., due to out-of-plane motion. The 20th percentile was chosen to deal with heartbeat-related motion, where we have about 10 frames per heartbeat. Using the 20th percentile ensures that the contrast spots, which might disappear in one or two frames per cardiac cycle, will still be preserved after the PerIP step. Although using PerIP instead of MinIP may preserve more u-MBs in cases of low number of frames or slow moving MBs [MBs labeled with 1 to 4 in Fig. 4(b)], the MB detection and tracking steps are able to distinguish them from truly stationary MBs.

In vitro, we showed that all the MBs after the MinIP and PerIP steps for the short sequence are detected and tracked correctly [see the complementary video file (🎞) which shows the tracking of all the detected contrast spots in Fig. 4(b) over all 10 frames]. Velocity of the moving MBs in our *in vitro* experiment was calculated to be around 0.8 mm/sec. This is a representative model for larger microvessels considering the velocity of red blood cells in mice tumor microvasculature (0.006 to 1.2 mm/sec [28]).

Although our quantification method successfully detected and tracked the MBs *in vitro*, it needed to be validated in a more complex *in vivo* condition. Therefore, the *in vivo* experiments on the murine tumor model were conducted ($n = 2$) (Fig. 6). In this model, the results of our method showed very good agreement with visual evaluation of the images and the classical approach (Fig. 7). Intensities in the subtracted MinIP and PerIP images for short and long sequences showed significant differences for the targeted and control injections in these subjects. As expected, PerIP was less sensitive to the length of the analyzed sequences. However, when MinIP was applied, in the longer sequence more contrast spots were missed in the images because of out-of-plane motion. Therefore, for our quantification method with the MinIP step, short sequences are more suitable. In the case of long sequences, the PerIP step performed better than the MinIP step. Although gated acquisition (e.g., ECG) can be applied in applications with more severe out-of-plane motion, it can introduce errors in tracking contrast spots because of its lower frame rate. These *in vivo* experiments showed that our quantification method is specific to the b-MBs in a complex *in vivo* environment.

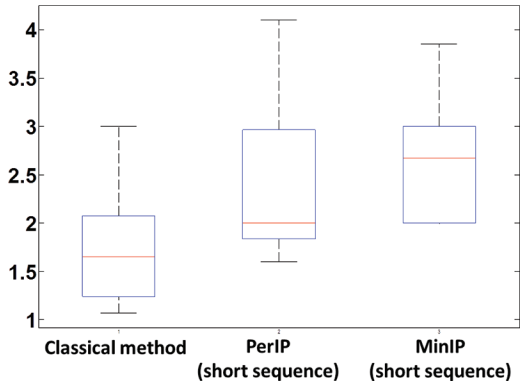

Fig. 9. Ratio of image intensities and ratio of number of detected bound microbubbles in targeted UCA injection versus control injection in the salivary gland of 7 mice.

The right salivary glands of 8 mice were scanned in the second *in vivo* experiment to test our method. Being right above the pulsating carotid, this target moves more than the tumor model. Quantification of the b-MBs with the classical approach in such a model is more difficult than the tumor model because of larger motion artifacts, less binding of the t-MBs, and more recirculating leftover MBs 10 min after injection. However, using our quantification method, sensitivity of the molecular imaging with t-MBs was improved for such a target (Figs. 8 and 9). The ratio of the intensity and number of detected b-MBs in targeted injections verssus the control injections were presented in Fig. 9 for 7 out of 8 scanned animals. One animal was discarded from the analysis because b-MBs were higher in the control injection than in the targeted injection (perhaps because of some leftover t-UCA in the injection tubes from the first injection). The result of our quantification method in this *in vivo* model for both the MinIP and PerIP approaches show higher ratios of targeted over control injection than the classical approach. Applying the MB detection and tracking steps on the subtracted MinIP images showed the highest average ratio for the targeted injection versus the control injection, although the absolute number of b-MBs was the highest when PerIP was applied. This is due to the fact that there are more b-MBs missed by the MinIP step than by the PerIP. Therefore, the number of detected bound MBs in the control injection will also be lower when MinIP is applied. Because the number of b-MBs in the control injection is often very low, a small change can increase such a ratio of detected MBs. This implies that the PerIP approach might be a better option for general applications.

There have been some studies proposing methods for selectively imaging the b-MBs in real time: utilizing an image-push-image sequence [22]; transmission at a low frequency and reception at a high frequency [29]; using subharmonic response of the MBs and interframe filtering [30]; and using singular value spectra properties [31]. However, none of the proposed methods in the mentioned publications have been applied in a complex *in vivo* condition. Only Pysz *et al.* on developed a quantification method based on dwell time MB signal measurements which was tested *in vivo* in well vascularized tumors in mice [32]. In such an *in vivo* model where attachment of t-MBs is significant, the classical way of quantification also performs well. Thus, the performance of the method developed by Pysz *et al.* in applications with very few t-MBs in presence of circulating MBs remains unclear. Our quantification method, on the other hand, has shown reliable detection of molecular signals *in vivo* in cases with many as well as very few b-MBs, although it is an offline image-processing method. Moreover, counting the b-MBs instead of reporting a sum of image intensities in the ROI implies that the result does not need to be adjusted for imaging parameters such as gain, dynamic range, attenuation, etc. This gives the opportunity to compare studies done with different ultrasound systems. Motion compensation, contrast detection, and tracking steps of our method have been validated previously (see [24] and [26]). However, the falsely detected and missed b-MBs in more complex *in vivo* conditions must be quantified more accurately than visual validation.

Our quantification methods have been validated for high-frequency ultrasound. Although high-frequency ultrasound has its limitation in clinical application because of the limited penetration depth, we believe our technique can also be applied on images acquired at lower frequencies because individual MBs can be imaged at frequencies as low as 7 MHz [33]. Another concern for the application of t-UCA in humans is the waiting time for freely floating MBs. The major factor to consider is therefore the half-life of MBs in the bloodstream. Definity (DuPont Pharmaceuticals, Bristol-Myers-Squibb, N. Billerica, MA, USA) and SonoVue (Bracco Diagnostic, Milano, Italy), both commercially available contrast agents for human use, have a half-life of ∼6 min [34], [35] which is similar to that in mice (∼7 min [36]). If targeted microbubbles based on these contrast agents have a similar half-life, a waiting time of 10 min would be sufficient.

V. Conclusion

A dedicated targeted ultrasound contrast agent quantification method has been developed to reliably detect individual contrast spots and classify them into bound and unbound microbubbles *in vitro* and *in vivo*. Because of the pre-processing steps such as motion compensation, minimum intensity projection, and 20th-percentile intensity projection, this technique should be more reliable and robust in different experimental conditions.

Acknowledgments

We greatly thank all colleagues who made the experiments possible for their help and support, especially S. van Tiel, G. Doeswijk, and M. Bernsen from the Department of Radiology, Erasmus MC, Rotterdam, The Netherlands; P. Leenders, A. Strzelecka, and J. Debets from the Department of Pharmacology, MUMC, Maastricht, The Netherlands; and T. Theelen and A. Janssen from the Department of Pathology, MUMC, Maastricht, the Netherlands.

References

[1] F. S. Foster, J. Hossack, and S. L. Adamson, "Micro-ultrasound for preclinical imaging," *Interface Focus*, vol. 1, no. 4, pp. 576–601, 2011.

[2] P. Carmeliet and R. K. Jain, "Angiogenesis in cancer and other diseases," *Nature*, vol. 407, no. 6801, pp. 249–257, 2000.

[3] M. M. Alauddin and J. G. Gelovani, "Radiolabeled nucleoside analogues for PET imaging of HSV1-tk gene expression," *Curr. Top. Med. Chem.*, vol. 10, no. 16, pp. 1617–1632, 2010.

[4] D. A. Sipkins, D. A. Cheresh, M. R. Kazemi, L. M. Nevin, M. D. Bednarski, and K. C. Li, "Detection of tumor angiogenesis in vivo by

alpha$_V$beta$_3$-targeted magnetic resonance imaging," *Nat. Med.*, vol. 4, no. 5, pp. 623–626, 1998.
[5] J. Li, A. Chaudhary, S. J. Chmura, C. Pelizzari, T. Rajh, C. Wietholt, M. Kurtoglu, and B. Aydogan, "A novel functional CT contrast agent for molecular imaging of cancer," *Phys. Med. Biol.*, vol. 55, no. 15, pp. 4389–4397, 2010.
[6] Q. Shao and B. Xing, "Photoactive molecules for applications in molecular imaging and cell biology," *Chem. Soc. Rev.*, vol. 39, no. 8, pp. 2835–2846, 2010.
[7] A. L. Klibanov, "Ligand-carrying gas-filled microbubbles: Ultrasound contrast agents for targeted molecular imaging," *Bioconjug. Chem.*, vol. 16, no. 1, pp. 9–17, 2005.
[8] B. A. Kaufmann, "Ultrasound molecular imaging of atherosclerosis," *Cardiovasc. Res.*, vol. 83, no. 4, pp. 617–625, 2009.
[9] H. Leong-Poi, J. Christiansen, A. L. Klibanov, S. Kaul, and J. R. Lindner, "Noninvasive assessment of angiogenesis by ultrasound and microbubbles targeted to alpha (v)-integrins," *Circulation*, vol. 107, no. 3, pp. 455–460, 2003.
[10] S. M. Stieger, P. A. Dayton, M. A. Borden, C. F. Caskey, S. M. Griffey, E. R. Wisner, and K. W. Ferrara, "Imaging of angiogenesis using Cadence contrast pulse sequencing and targeted contrast agents," *Contrast Media Mol. Imaging*, vol. 3, no. 1, pp. 9–18, 2008.
[11] P. Hauff, M. Reinhardt, A. Briel, N. Debus, and M. Schirner, "Molecular targeting of lymph nodes with L-selectin ligand-specific US contrast agent: A feasibility study in mice and dogs," *Radiology*, vol. 231, no. 3, pp. 667–673, 2004.
[12] J. R. Lindner, "Contrast ultrasound molecular imaging of inflammation in cardiovascular disease," *Cardiovasc. Res.*, vol. 84, no. 2, pp. 182–189, 2009.
[13] G. L. ten Kate, E. J. Sijbrands, R. Valkema, F. J. ten Cate, S. B. Feinstein, A. F. van der Steen, M. J. Daemen, and A. F. Schinkel, "Molecular imaging of inflammation and intraplaque vasa vasorum: A step forward to identification of vulnerable plaques?" *J. Nucl. Cardiol.*, vol. 17, no. 5, pp. 897–912, 2010.
[14] G. M. Lanza, K. D. Wallace, M. J. Scott, W. P. Cacheris, D. R. Abendschein, D. H. Christy, A. M. Sharkey, J. G. Miller, P. J. Gaffney, and S. A. Wickline, "A novel site-targeted ultrasonic contrast agent with broad biomedical application," *Circulation*, vol. 94, no. 12, pp. 3334–3340, 1996.
[15] J. R. Lindner, "Microbubbles in medical imaging: Current applications and future directions," *Nat. Rev. Drug Discov.*, vol. 3, no. 6, pp. 527–532, 2004.
[16] A. L. Klibanov, J. J. Rychak, W. C. Yang, S. Alikhani, B. Li, S. Acton, J. R. Lindner, K. Ley, and S. Kaul, "Targeted ultrasound contrast agent for molecular imaging of inflammation in high-shear flow," *Contrast Media Mol. Imaging*, vol. 1, no. 6, pp. 259–266, 2006.
[17] P. A. Dayton and K. W. Ferrara, "Targeted imaging using ultrasound," *J. Magn. Reson. Imaging*, vol. 16, no. 4, pp. 362–377, 2002.
[18] M. Palmowski, J. Huppert, G. Ladewig, P. Hauff, M. Reinhardt, M. M. Mueller, E. C. Woenne, J. W. Jenne, M. Maurer, G. W. Kauffmann, W. Semmler, and F. Kiessling, "Molecular profiling of angiogenesis with targeted ultrasound imaging: Early assessment of antiangiogenic therapy effects," *Mol. Cancer Ther.*, vol. 7, no. 1, pp. 101–109, 2008.
[19] M. Piedra, A. Allroggen, and J. R. Lindner, "Molecular imaging with targeted contrast ultrasound," *Cerebrovasc. Dis.*, vol. 27, suppl 2, pp. 66–74, 2009.
[20] P. Dayton and J. J. Rychak, "Molecular ultrasound imaging using microbubble contrast agents," *Front. Biosci.*, vol. 12, pp. 5124–5142, 2007.
[21] C. R. Anderson, X. Hu, H. Zhang, A. E. Declèves, R. Houghtaling, K. Sharma, M. Lawrence, K. W. Ferrara, and J. J. Rychak, "Ultrasound molecular imaging of tumor angiogenesis with an integrin targeted microbubble contrast agent," *Invest. Radiol.*, vol. 46, no. 4, pp. 215–224, 2011.
[22] S. Zhao, D. E. Kruse, K. W. Ferrara, and P. A. Dayton, "Selective imaging of adherent targeted ultrasound contrast agents," *Phys. Med. Biol.*, vol. 52, no. 8, pp. 2055–2072, 2007.
[23] A. Needles, M. Arditi, N. G. Rognin, J. Mehi, T. Coulthard, C. Bilan-Tracey, E. Gaud, P. Frinking, D. Hirson, and F. S. Foster, "Nonlinear contrast imaging with an array based micro-ultrasound system," *Ultrasound Med. Biol.*, vol. 36, no. 12, pp. 2097–2106, 2010.
[24] Z. Akkus, A. Hoogi, G. Renaud, G. L. ten Kate, S. C. H. van den Oord, A. F. L. Schinkel, N. de Jong, A. F. W. van der Steen, and J. G. Bosch, "Motion compensation method using dynamic programming for quantification of neovascularization in carotid atherosclerotic plaques with contrast enhanced ultrasound (CEUS)," *Proc. SPIE*, vol. 8320, art. no. 83200C, 2012.
[25] M. Üzümcü, R. J. Van der Geest, C. Swingen, J. H. Reiber, and B. P. Lelieveldt, "Time continuous tracking and segmentation of cardiovascular magnetic resonance images using multidimensional dynamic programming," *Invest. Radiol.*, vol. 41, no. 1, pp. 52–62, 2006.
[26] A. Hoogi, Z. Akkus, S. C. H. van den Oord, G. L. ten Kate, A. F. Schinkel, J. G. Bosch, N. de Jong, D. Adam, and A. F. van der Steen, "Quantitative analysis of ultrasound contrast flow behavior in carotid plaque neovasculature," *Ultrasound Med. Biol.*, vol. 38, no. 12, pp. 2072–2083, 2012.
[27] C. J. Teirlinck, R. A. Bezemer, C. Kollmann, J. Lubbers, P. R. Hoskins, K. V. Ramnarine, P. Fish, K. E. Fredeldt, and U. G. Schaarschmidt, "Development of an example flow test object and comparison of five of these test objects, constructed in various laboratories," *Ultrasonics*, vol. 36, no. 1–5, pp. 653–660, 1998.
[28] M Leunig, F Yuan, MD Menger, Y Boucher, AE Goetz, K Messmer, and RK Jain, "Angiogenesis, microvascular architecture, microhemodynamics, and interstitial fluid pressure during early growth of human adenocarcinoma LS174T in SCID mice," *Cancer Res.*, vol. 52, no. 23, pp. 6553–6560, 1992.
[29] X. Hu, H. Zheng, D. E. Kruse, P. Sutcliffe, D. N. Stephens, and K. W. Ferrara, "A sensitive TLRH targeted imaging technique for ultrasonic molecular imaging," *IEEE Trans. Ultrason. Ferroelectr. Freq. Control*, vol. 57, no. 2, pp. 305–316, 2010.
[30] A. Needles, O. Couture, and F. S. Foster, "A method for differentiating targeted microbubbles in real time using subharmonic micro-ultrasound and interframe filtering," *Ultrasound Med. Biol.*, vol. 35, no. 9, pp. 1564–1573, 2009.
[31] F. W. Mauldin Jr., A. H. Dhanaliwala, A. V. Patil, and J. A. Hossack, "Real-time targeted molecular imaging using singular value spectra properties to isolate the adherent microbubble signal," *Phys. Med. Biol.*, vol. 57, no. 16, pp. 5275–5293, 2012.
[32] M. A. Pysz, I. Guracar, L. Tian, and J. K. Willmann, "Fast microbubble dwell-time based ultrasonic molecular imaging approach for quantification and monitoring of angiogenesis in cancer," *Quant. Imaging Med. Surg.*, vol. 2, no. 2, pp. 68–80, 2012.
[33] A. L. Klibanov, P. T. Rasche, M. S. Hughes, J. K. Wojdyla, K. P. Galen, J. H. J. Wible, and G. H. Brandenburger, "Detection of individual microbubbles of ultrasound contrast agents: Imaging of free-floating and targeted bubbles," *Invest. Radiol.*, vol. 39, no. 3, pp. 187–195, 2004.
[34] M. Schneider, "Characteristics of SonoVue (TM)," *Echocardiography*, vol. 16, no. 7, pp. 743–746, 1999.
[35] D. W. Kitzman, M. E. Goldman, L. D. Gillam, J. L. Cohen, G. P. Aurigemma, and J. S. Gottdiener, "Efficacy and safety of the novel ultrasound contrast agent Perflutren (Definity) in patients with suboptimal baseline left ventricular echocardiographic images," *Am. J. Cardiol.*, vol. 86, no. 6, pp. 669–674, 2000.
[36] D. S. Wang, C. Panje, M. A. Pysz, R. Paulmurugan, J. Rosenberg, S. S. Gambhir, M. Schneider, and J. K. Willmann, "Cationic versus neutral microbubbles for ultrasound-mediated gene delivery in cancer," *Radiology*, vol. 264, no. 3, pp. 721–732, 2012.

Verya Daeichin was born in Kermanshah, Iran, in 1984. He received the bachelor's degree in bioelectric engineering from the Biomedical Engineering Department at Amirkabir University of Technology (Tehran Polytechnic) in 2008. In 2009, he finished his first master's degree in biomedical signal processing and pattern recognition from University of Boras in Sweden. His second master's degree was from Chalmers University of Technology in biomedical image processing. Since 2010, he has been a Ph.D. candidate at Erasmus MC, Rotterdam, The Netherlands. His research area is molecular imaging using target microbubbles contrast agents.

Zeynettin Akkus received his M.Sc. degree in medical imaging from the Medical Engineering Department of the School of Health and Technology, KTH, the Royal Institute of Technology, Stockholm, Sweden, in 2009. He worked as a visiting researcher in the Ultrasound Research Group, Department of Medical Physics, University Hospitals of Leicester, Royal Infirmary, in 2009. He has been working as a junior researcher (Ph.D. student) in the Biomedical Engineering Department, Erasmus Medical Center, Rotterdam, The Netherlands, since 2010. His research interests are biomedical image and signal processing, angiogenesis imaging and quantification, and photoacoustic imaging. He received the Best Paper Award in 2013 from the IEEE Ultrasonics Symposium and the Best Poster Award in 2013 from the 18th European Symposium on Ultrasound Contrast Imaging.

Ilya Skachkov studied at the Faculty of Biology at Lomonosov Moscow State University in Russia and obtained his degree from the Department of Cell Biology and Histology in 2009. From 2009 to 2010, he was working in Institute for Biomedical Problems studying molecular pathways involved in muscle degeneration in response to hypogravity. In 2010, he joined the Department of Biomedical Engineering of the Thorax Centre, Erasmus MC, as a Ph.D. student, where he still works. His main research topics are ultrasound contrast agents for molecular imaging and drug delivery and revealing mechanisms of sonoporation.

Klazina Kooiman (M'12) studied bio-pharmaceutical sciences at Leiden University, the Netherlands, and obtained her M.Sc. degree cum laude specializing in pharmaceutical technology. From 2005 to 2010, she was a Ph.D. student in the Department of Biomedical Engineering of the Thorax Centre, Erasmus MC, The Netherlands. On January 19, 2011, she obtained her Ph.D. degree on the topic of ultrasound contrast agents for therapy. She currently holds a postdoctoral position in the Department of Biomedical Engineering of the Thorax Centre, Erasmus MC, focusing on using ultrasound contrast agents for drug delivery and molecular imaging. At EFUSMB 2011 in Vienna, she won the young investigator award. She was awarded the ICIN Fellowship 2012, which enabled her to perform research for seven months in 2012 to 2013 in the lab of Professor F. S. Villanueva, director of the Center for Ultrasound Molecular Imaging and Therapy at UPMC, Pittsburgh, PA, USA.

Andrew Needles received his B.A.Sc. degree in electrical engineering from the University of Toronto, ON, Canada, in May 2002. During his studies, he participated in a 16-month internship at JDS Uniphase Inc., Ottawa, ON, where he worked on the development of instrumentation used for manufacturing and testing fiber-optic components. After graduation, he began working as a Research Engineer at Sunnybrook Health Sciences Centre, Toronto, in the Department of Imaging Research. His research focused on the use of high-frequency ultrasound (>20 MHz) for imaging blood flow in microcirculation. In 2007, he became a Systems Developer with VisualSonics Inc., Toronto, developing high-frequency ultrasound and photoacoustic imaging systems. Currently, he is a Senior Manager of Product Innovation with FUJIFILM VisualSonics Inc. and is responsible for all ultrasound and photoacoustic imaging product lines. His research interests include Doppler signal processing, microbubble contrast agent behavior and detection, as well as photoacoustic imaging and optical contrast agents.

Judith Sluimer graduated in 2000 from Maastricht University with a Master of Science degree in Health Sciences. After a 2-year appointment as clinical research manager at the Orthopaedics department of Maastricht University Medical Center (MUMC), she started a Ph.D. project with Prof. Mat Daemen in the Pathology Department of Maastricht University. She established the first proof of hypoxia in human and murine atherosclerosis and investigated the hypoxia-dependent formation and leaky phenotype of atherosclerotic plaque angiogenesis. After her Ph.D. defense, she joined the lab of Prof. Ira Tabas (Columbia University, NYC) in 2008 as a postdoctoral fellow. This fellowship was supported by grants from the Netherlands Scientific Organisation (NWO, Rubicon), the international atherosclerosis society (IAS), and Maastricht University (Kootstra talent award). Since the end of 2009, she has been studying the functional role of hypoxia and leaky angiogenesis in atherosclerosis in the department of Pathology of Maastricht University Medical Center. In 2010, she acquired the VENI grant from NWO to investigate pharmaceutical and genetic strategies to improve plaque oxygen levels and their impact on atherogenesis. In addition, she is assessing the potential of noninvasive imaging of human plaque hypoxia and angiogenesis to predict plaque rupture in the CTMM-funded "plaque at risk" (PARISK) initiative (Prof. Daemen, AMC, and Prof van der Steen, ErasmusMC).

Ben J. A. Janssen is an Associate Professor of Pharmacology and staff member at the Department of Pharmacology of the Maastricht University. He received his M.Sc. degree in biology from the University of Nijmegen in 1983. In 1988, he received his Ph.D. degree from Maastricht University for his thesis "Sensory renal nerves and hypertension." Since then, he has been head of the experimental animal laboratory of the Department of Pharmacology and has been involved in the technical development of invasive and noninvasive techniques to phenotype animal models used in cardiovascular research, including hypertension, atherosclerosis, and heart failure. In 1995, he was a visiting senior scientist at the Neuropharmacology laboratory of Prof. J. Head at the Baker Medical Research Institute, Melbourne, Australia, where he specialized in assessing autonomic nervous activity measurement from cardiovascular signals. He is co-author of more than 120 peer-reviewed papers and was involved in setting up experimental studies in a number of projects funded within the national Dutch TIPHARMA and CTMM initiatives. His current research interest on mechanism of early renal inflammation in hypertension. Additionally, he is teaching coordinator of the pharmacotherapy program at the Maastricht University.

Mat Daemen's photograph and biography were unavailable at time of publication.

A. F. W. (Ton) van der Steen (M'94–SM'03–F'13) is Professor in Biomedical Engineering in Cardiology. He received an M.Sc. degree in applied physics in 1989 from the Technical University Delft and a Ph.D. degree in medical science in 1994 from the Catholic University Nijmegen. Since 1994, he has been connected to the Thorax Centre and the Interuniversity Cardiology Institute of the Netherlands. He is head of Biomedical Engineering of the Thorax Centre, ErasmusMC. Since 2013, he has also been full professor in Applied Physics at the Technical University Delft. Since 2014, he has been honorary visiting professor to the Shenzhen Institutes of Advanced Technologies. His expertise is mainly in diagnostic cardiologic imaging devices, with emphasis on echography. Current research interests are focused on vulnerable atherosclerotic plaque detection, ultrasound contrast

agents, ultrasound transducers, and vascular biomechanics. His research on vulnerable plaque detection has resulted in many publications and several patents on IVUS flow, IVUS palpography, harmonic IVUS, and vasa vasorum detection. He is a member of the Netherlands Academy of Engineering (AcTI) and a member of the Netherlands Academy of Sciences (KNAW). He is a Fellow of the IEEE and a Fellow of the European Society of Cardiology. He was the IEEE UFFC Distinguished lecturer for 2011–2012

Nico de Jong (AM' 94) graduated from the Delft University of Technology, The Netherlands, in 1978. He received his M.Sc. degree in physics, specialized in the field of pattern recognition. Since 1980, he has been a staff member of the Thoraxcenter of the Erasmus Medical Center, Rotterdam. In 1993, he received his Ph.D. degree for "Acoustic properties of ultrasound contrast agents." In 2003, he became a part-time professor at the University of Twente in the group Physics of Fluids headed by Detlef Lohse (Spinoza winner, 2005). He is organizer of the annual European Symposium on Ultrasound Contrast Imaging, held in Rotterdam and attended by approximately 175 scientists from universities and industries all over the world. He is on the safety committee of the World Federation of Ultrasound in Medicine and Biology (WFUMB), associate editor of UMB, and has been guest editor for special issues of different journals. Over the last 5 years, he has given more than 30 invited lectures and has given numerous scientific presentations for international industries. He teaches at Technical Universities and the ErasmusMC. He has been Promotor of 15 Ph.D. students and is currently supervising 9 Ph.D. students. Since October 1, 2011, he has been professor in Molecular Ultrasonic Imaging and Therapy at the ErasmusMC and the Technical University of Delft. He has published more than 180 peer reviewed articles and has an H-index of 41.

Johan G. Bosch (M'07) is an Associate Professor and staff member at the Department of Biomedical Engineering, Thoraxcenter, Erasmus MC, Rotterdam. He specializes in 2-D and 3-D echocardiographic image processing/analysis and transducer development. His main research interests are optimal border detection approaches, geometrical and statistical models, and anatomical and physical knowledge representations for border detection. He is currently leader of projects on 3-D segmentation and 3-D ultrasound guidance in electrophysiology and participates in several projects, e.g. on 3-D transducer development, 2-D and 3-D carotid imaging, and 3-D TEE imaging. He obtained his M.Sc. degree in electrical engineering at the Eindhoven University of Technology in 1985. He performed ultrasound and image processing research at Erasmus University Rotterdam and Leiden University. From 1995–2005, he was Assistant Professor and head of the Echocardiography section at the Division of Image Processing (LKEB), Department of Radiology, Leiden University Medical Center, where he obtained his Ph.D. degree in 2006.